Database of normal human cerebral blood flow measured by SPECT: I. Comparison between I-123-IMP, Tc-99m-HMPAO, and Tc-99m-ECD as referred with O-15 labeled water PET and voxel-based morphometry

Hiroshi Ito,*,** Kentaro Inoue,* Ryoi Goto,* Shigeo Kinomura,* Yasuyuki Taki,* Ken Okada,*
Kazunori Sato,* Tachio Sato,* Iwao Kanno*** and Hiroshi Fukuda*

*Department of Nuclear Medicine and Radiology,
Institute of Development, Aging and Cancer, Tohoku University
**Brain Imaging Project, National Institute of Radiological Sciences
***Department of Radiology and Nuclear Medicine,
Akita Research Institute of Brain and Blood Vessels

Objectives: Three accumulative tracers, iodine-123-labeled N-isopropyl-p-iodoamphetamine (I-123-IMP), technetium-99m-labeled hexamethylpropyleneamineoxime (Tc-99m-HMPAO), and technetium-99m-labeled ethyl cysteinate dimer (Tc-99m-ECD) are widely used to measure cerebral blood flow (CBF) in single-photon emission computed tomography (SPECT). In the present study, normal regional distribution of CBF measured with three different SPECT tracers was entered into a database and compared with regional distribution of CBF measured by positron emission tomography (PET) with $H_2^{15}O$. The regional distribution of tissue fractions of gray matter determined by voxel-based morphometry was also compared with SPECT and PET CBF distributions. **Methods:** SPECT studies with I-123-IMP, Tc-99m-HMPAO, and Tc-99m-ECD were performed on 11, 20, and 17 healthy subjects, respectively. PET studies were performed on 11 healthy subjects. Magnetic resonance (MR) imaging studies for voxel-based morphometry were performed on 43 of the 48 subjects who underwent SPECT study. All SPECT, PET, and MR images were transformed into the standard brain format with the SPM2 system. The voxel values of each SPECT and PET image were globally normalized to 50 ml/100 ml/min. Gray matter, white matter, and cerebrospinal fluid images were segmented and extracted from all transformed MR images by applying voxel-based morphometry methods with the SPM2 system. **Results:** Regional distribution of all three SPECT tracers differed from that of $H_2^{15}O$ in the pons, midbrain, thalamus, putamen, parahippocampal gyrus, posterior cingulate gyrus, temporal cortex, and occipital cortex. No significant correlations were observed between the tissue fraction of gray matter and CBF with any tracer. **Conclusion:** Differences in regional distribution of SPECT tracers were considered to be caused mainly by differences in the mechanism of retention of tracers in the brain. Regional distribution of CBF was independent of regional distribution of gray matter fractions, and consequently the blood flow per gray matter volume differed for each brain region.

Key words: SPECT, CBF, I-123-IMP, Tc-99m-HMPAO, Tc-99m-ECD

INTRODUCTION

DIFFUSIBLE TRACERS, such as $H_2^{15}O$ or ^{133}Xe, can be used to measure regional cerebral blood flow (CBF) with positron emission tomography (PET) and single-photon emission computed tomography (SPECT) due to their large first-pass extraction fraction in the brain tissue.[1–3]

Three accumulative radioligands, iodine-123-labeled *N*-isopropyl-*p*-iodoamphetamine (IMP),[4,5] technetium-99m-labeled hexamethylpropyleneamineoxime (PAO),[6,7] and technetium-99m-labeled ethyl cysteinate dimer (ECD),[8,9] have been developed for use as CBF tracers for SPECT and have been used to investigate the pathophysiology of several neurological diseases. These three radioligands all have a large first-pass extraction fraction in brain tissue; however, the mechanism of retention in the brain is different for each radioligand. IMP binds to amine-binding sites in brain tissue.[4] PAO is retained by interaction of the lipophilic complex with glutathione in brain tissue.[10] ECD is retained due to metabolic transformation into its acid products by the enzymatic system in brain tissue.[11] These differences in the mechanism of retention must cause differences in regional distribution in the brain, although all three radioligands are used as CBF tracers. Differences in regional distribution of PAO and ECD have been reported.[12,13] However, there has been no investigation comparing regional distribution of IMP, PAO, and ECD in SPECT assessments of CBF to the distribution of $H_2^{15}O$ in PET assessments of CBF.

It has been reported that blood flow in gray matter is four to five times greater than that in white matter.[14–18]

Therefore, the regional difference in tissue fractions of gray and white matter in a region-of-interest must relate to the regional difference in CBF. A voxel-based morphometry technique, in which gray matter, white matter, and cerebrospinal fluid images are segmented and extracted from magnetic resonance (MR) images,[19] has recently been developed. This technique has been used to investigate regional cerebral volume and tissue concentration in terms of age, sex, and other patient characteristics.[20,21]

In the present study, regional distribution of IMP, PAO, and ECD in SPECT studies of CBF was compared to regional distribution of $H_2^{15}O$ in PET studies of CBF. Regional differences in tissue fractions of gray and white matter obtained by voxel-based morphometry were also compared.

MATERIALS AND METHODS

Subjects
A total of 59 healthy subjects were recruited and gave written informed consent to participate in the study (Table 1). The subjects were judged healthy on the basis of their medical history, a physical examination, and MR imaging or X-ray computed tomography of the brain. The study was approved by the Ethics Committees of the Institute of Development, Aging and Cancer, Tohoku University, and the Akita Research Institute of Brain and Blood Vessels. Each subject underwent only one study of SPECT or PET.

SPECT procedures
The SPECT study was performed in 48 subjects: with IMP in 11, PAO in 20, and ECD in 17 subjects. A SPECT scanner (SPECT-2000H, Hitachi Medico Corp., Tokyo, Japan)[22] with a four-head rotating gamma camera was used for all SPECT studies. For the IMP study, fitted

**Table 1** Number of subjects per study and their average age

Study	Number of subjects		Age (y, mean ± SD)
	Male	Female	
PET	11	0	58.1 ± 4.5
SPECT			
IMP	5	6	61.6 ± 6.7
PAO	10	10	57.0 ± 5.4
ECD	10	7	57.1 ± 4.0
MRI	23	20	58.4 ± 5.6

Table 2 Average CBF values for each ROI (ml/100 ml/min)

| Region	PET	SPECT		
		IMP	PAO	ECD
Cerebellum	64.9 ± 7.0	64.1 ± 2.4	65.0 ± 1.9	64.3 ± 2.2
Pons	55.7 ± 8.0	50.5 ± 2.5	50.6 ± 1.8†	47.8 ± 2.1*
Midbrain	54.3 ± 3.5	47.6 ± 3.6*	50.0 ± 1.6*	44.8 ± 2.0*
Thalamus	66.7 ± 6.2	53.9 ± 2.9*	58.5 ± 1.8*	52.5 ± 1.9*
Putamen	67.8 ± 4.1	59.2 ± 2.0*	62.1 ± 1.7*	59.6 ± 2.0*
Parahippocampal gyrus	53.4 ± 3.4	50.1 ± 2.6‡	54.1 ± 1.2	46.8 ± 1.2*
Anterior cingulate	51.6 ± 3.7	50.9 ± 2.3	53.0 ± 2.0	50.6 ± 1.1
Posterior cingulate	62.4 ± 4.2	53.5 ± 2.4*	55.6 ± 1.6*	53.6 ± 1.9*
Frontal cortex	51.9 ± 2.7	53.6 ± 2.7	53.2 ± 1.6	51.4 ± 1.2
Temporal cortex	63.5 ± 3.5	58.2 ± 1.7*	56.3 ± 2.1*	55.9 ± 1.1*
Occipital cortex	66.1 ± 4.0	60.7 ± 2.0*	58.9 ± 2.2*	64.2 ± 1.2
Parietal cortex	54.3 ± 2.5	53.8 ± 2.9	53.5 ± 1.3	52.9 ± 1.2
Centrum semiovale	32.9 ± 1.3	37.8 ± 1.9*	38.0 ± 1.4*	33.6 ± 1.4

Values are shown as mean ± SD
Significant differences from PET values (two sample t-test): *p < 0.001, †p < 0.01, ‡p < 0.05
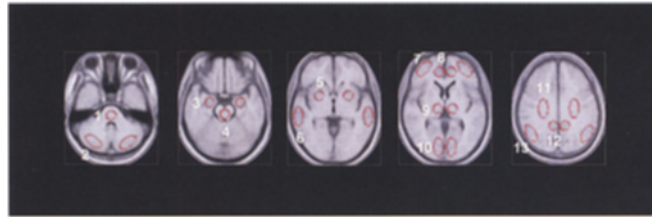
Fig. 1 Regions of interest drawn on all anatomically standardized images (1: pons, 2: cerebellum, 3: parahippocampal gyrus, 4: midbrain, 5: putamen, 6: temporal cortex, 7: frontal cortex, 8: anterior part of the cingulate gyrus, 9: thalamus, 10: occipital cortex, 11: centrum semiovale, 12: posterior part of the cingulate gyrus, 13: parietal cortex). All images are transaxial sections parallel to the anterior-posterior commissure (AC-PC) line. The slice positions are −36, −18, 0, 6, and 36 mm from the AC-PC line.
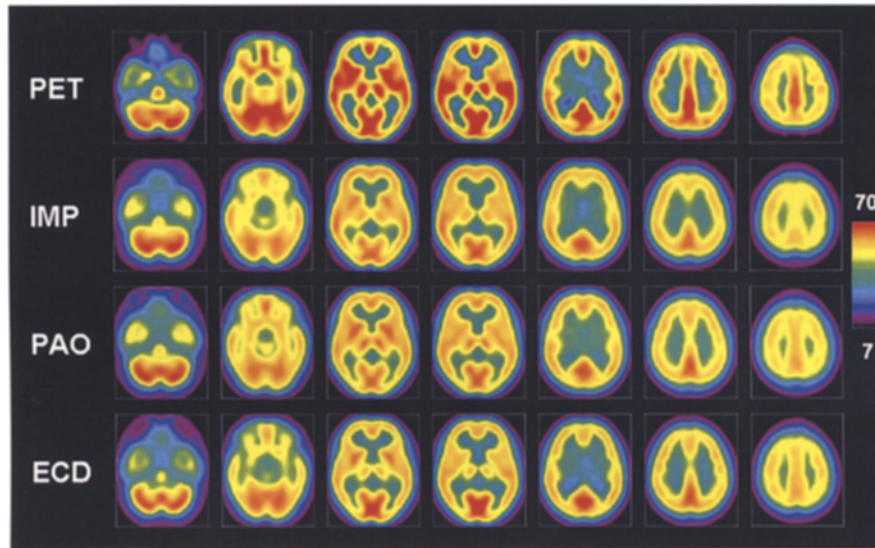
Fig. 2 Anatomically standardized averaged CBF images obtained with PET and SPECT (IMP, PAO, and ECD). All images are transaxial sections parallel to the AC-PC line. The slice positions are −36, −18, 0, 6, 22, 36, and 50 mm from the AC-PC line. Scale maximum and minimum values for all images are 70 and 7 ml/100 ml/min, respectively.
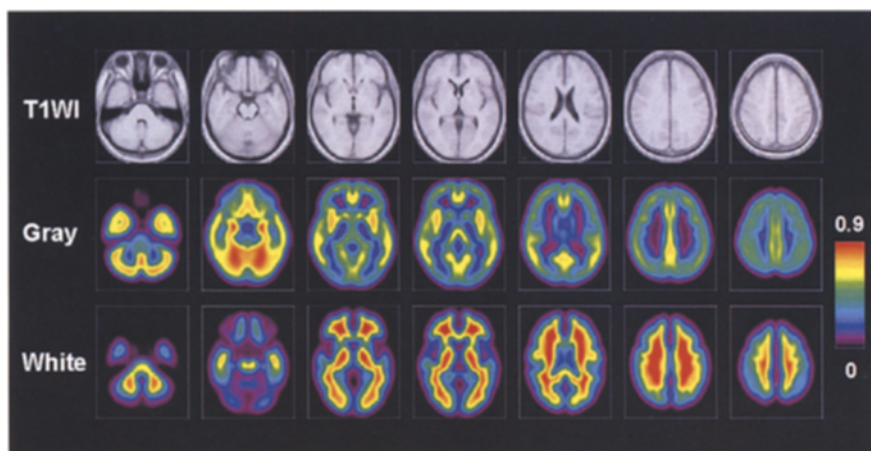
Fig. 3 Anatomically standardized averaged T1-weighted MR images and averaged images of gray and white matter fractions. All images are transaxial sections parallel to the AC-PC line. The slice positions are −36, −18, 0, 6, 22, 36, and 50 mm from the AC-PC line. Scale maximum and minimum values for gray and white matter images are 0.9 and 0 ml/ml, respectively. T1WI, T1-weighted image.
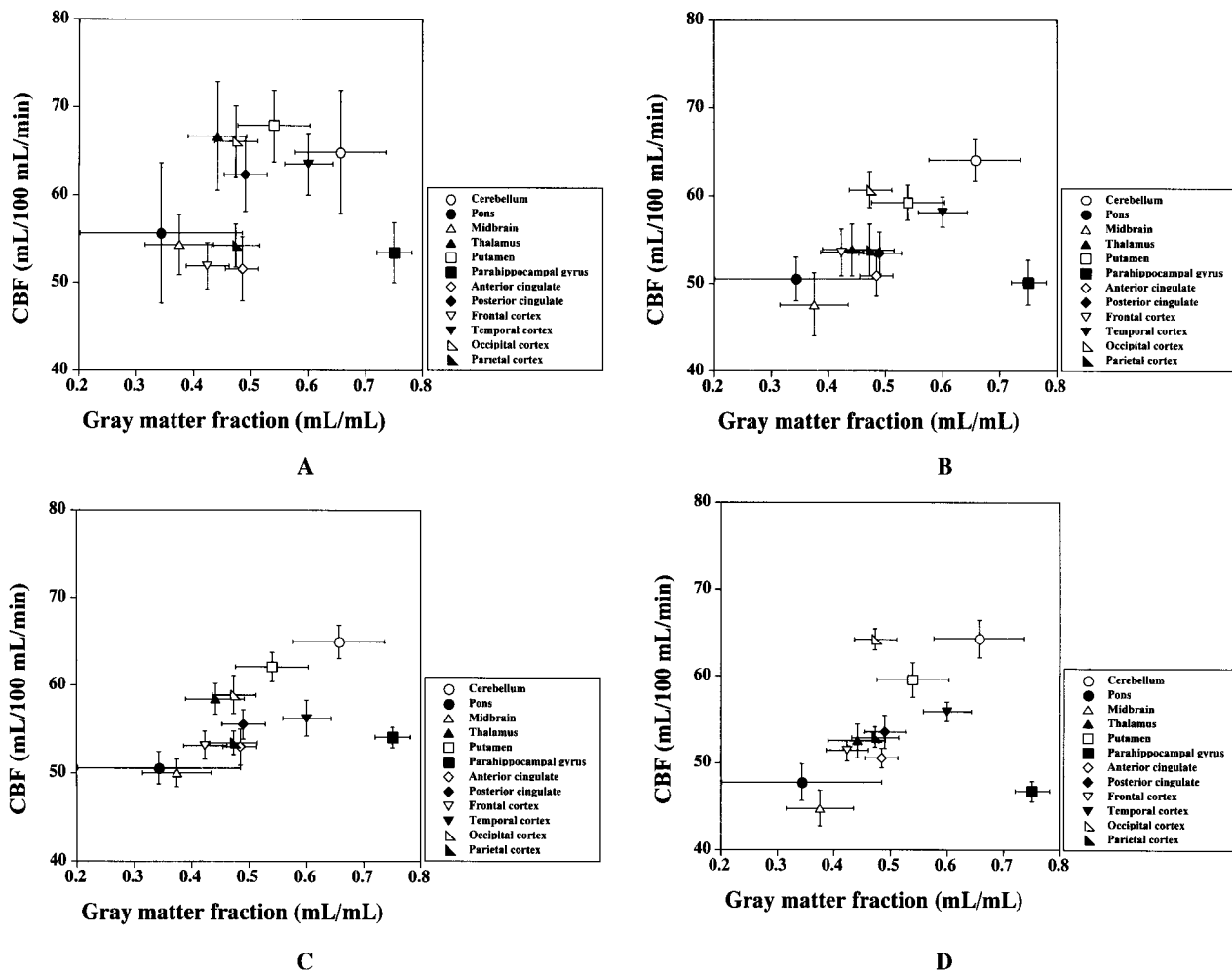
Fig. 4 Relations between average tissue fraction of gray matter and average CBF values obtained with PET or SPECT for all ROIs. (A) Relation between average tissue fraction of gray matter and average CBF values on PET. (B) Relation between average tissue fraction of gray matter and average CBF values on SPECT with IMP. (C) Relation between average tissue fraction of gray matter and average CBF values on SPECT with PAO. (D) Relation between average tissue fraction of gray matter and average CBF values on SPECT with ECD.

collimator was low-energy, medium-resolution, and in-plane and axial resolutions of 10 mm full width at half maximum (FWHM). For PAO and ECD studies, fitted collimator was low-energy, high-resolution, and in-plane and axial resolutions of 8 mm FWHM. Image reconstruction was performed by filtered backprojection with a Butterworth filter, and attenuation correction was made numerically by assuming the object shape to be an ellipse for each slice and the attenuation coefficient to be uniform (0.08 cm^{-1} for IMP; 0.1 cm^{-1} for PAO and ECD).[23,24] Correction for scattered photons was not performed. Image slices were set up parallel to the orbito-meatal line and were obtained through the whole brain.

For the IMP study, the SPECT scanning was performed at 40 min of mid-scan time after intravenous infusion of 111 MBq IMP for 1 min. The SPECT scan protocol acquired 64 projections at 25 sec (25 sec × 4 camera heads = 100 sec total) per projection with 360° continuous

rotation of the camera. For PAO and ECD studies, the SPECT scanning was performed 5–10 min after intravenous bolus injection of 740 MBq PAO or 740 MBq ECD. The SPECT protocol comprised 64 projections at 20 sec (20 sec × 4 camera heads = 80 sec total) per projection with 360° rotation of the camera. No quantitative analyses for determination of CBF were performed on all SPECT data.

PET procedures

PET was performed in 11 subjects. The Headtome-V PET system (Shimadzu Corp., Kyoto, Japan) used for all PET studies provides 47 slices with center-to-center distances of 3.125 mm.[25] The intrinsic spatial resolution is 4.0 mm in plane and 4.3 mm FWHM axially. Reconstruction with a Butterworth filter resulted in a final in-plane resolution of approximately 8 mm FWHM. Data were acquired in the two-dimensional mode.

The H$_2$^{15}O PET study was performed after transmis-

sion scanning. The protocol consisted of 180-sec static scanning following continuous intravenous infusion of $H_2{}^{15}O$ for 2 min. The arterial input function was determined with a beta probe for continuous measurement of arterial whole blood radioactivity. Dispersion and delay occurring in the beta detector system and in the internal arterial line were corrected according to previously reported methods.[26,27] The CBF images were calculated by an autoradiographic method.[3,28]

MR imaging procedures

All MR imaging studies were performed with a 0.5-Tesla MR scanner (GE, Milwaukee, WI). Three-dimensional volumetric acquisition of a T1-weighted gradient echo sequence produced a gapless series of thin transverse sections under SPGR sequencing (TE: 7 msec; TR: 40 msec; flip angle: 30°; field of view: 25 cm; acquisition matrix: 256 × 256; slice thickness: 1.5 mm). MR imaging study was performed in six of the 11 subjects who underwent SPECT study with IMP and in all subjects who underwent SPECT study with PAO or ECD.

Data analysis

All SPECT, PET, and MR images were transformed into the standard brain size and shape by linear and nonlinear parameters with the statistical parametric mapping (SPM2) system for anatomic standardization.[29] Used brain templates in SPM2 for anatomic standardization were PET template for all SPECT and PET images and T1 template for MR images. Thus, brain images of all subjects had the same anatomic format. The radioactivities of each SPECT image were globally normalized to 50 ml/100 ml/min with the use of whole brain radioactivities. The CBF values of PET images were also globally normalized to 50 ml/100 ml/min using whole brain CBF. Gray matter, white matter, and cerebrospinal fluid images were segmented and extracted from all anatomically standardized MR images by applying voxel-based morphometry methods with the SPM2 system.[19] These segmented MR images indicate the tissue fraction of gray or white matter per voxel (ml/ml). All anatomically standardized SPECT, PET, gray matter, and white matter images were smoothed with a 10-mm FWHM isotropic Gaussian kernel.

Regions of interest (ROIs) were drawn on all anatomically standardized SPECT, PET, gray matter, and white matter images with reference to the T1-weighted MR image (Fig. 1). Circular ROIs were defined for the pons, midbrain, thalamus, putamen, parahippocampal gyrus, and anterior and posterior parts of the cingulate gyrus (16 mm in diameter), and elliptical ROIs were defined for the cerebellar cortex, centrum semiovale, and four neocortical regions representing the frontal, temporal, occipital, and parietal lobes (16 mm × 32 mm).

Table 3 Average tissue fractions of gray and white matter per voxel (ml/ml)

Region	Tissue fraction	
	Gray matter	White matter
Cerebellum	0.657 ± 0.080	0.284 ± 0.088
Pons	0.344 ± 0.142	0.587 ± 0.144
Midbrain	0.375 ± 0.060	0.521 ± 0.068
Thalamus	0.441 ± 0.051	0.482 ± 0.052
Putamen	0.540 ± 0.063	0.451 ± 0.063
Parahippocampal gyrus	0.751 ± 0.030	0.144 ± 0.027
Anterior cingulate	0.484 ± 0.030	0.409 ± 0.030
Posterior cingulate	0.491 ± 0.038	0.440 ± 0.049
Frontal cortex	0.424 ± 0.037	0.426 ± 0.050
Temporal cortex	0.601 ± 0.042	0.272 ± 0.041
Occipital cortex	0.474 ± 0.037	0.423 ± 0.049
Parietal cortex	0.473 ± 0.042	0.414 ± 0.040
Centrum semiovale	0.051 ± 0.013	0.937 ± 0.016

Values are shown as mean ± SD

RESULTS

Average CBF values for PET and SPECT (IMP, PAO, and ECD) for each ROI are given in Table 2. In the midbrain, thalamus, putamen, posterior cingulate gyrus, and temporal cortex, CBF values were significantly lower in SPECT (IMP, PAO, and ECD) than in PET. In the pons, CBF values were significantly lower with PAO and ECD than with PET. In the parahippocampal gyrus, CBF values were significantly lower with IMP and ECD than with PET. In the occipital cortex, CBF values were significantly lower with IMP and PAO than with PET. Averaged PET and SPECT (IMP, PAO, and ECD) images of CBF that were anatomically standardized are shown in Figure 2.

Average tissue fractions of gray and white matter for each ROI are given in Table 3. Among the neocortical regions, the tissue fraction of gray matter in an ROI ranged from 0.424 to 0.601 ml/ml, whereas the tissue fraction of white matter ranged from 0.272 to 0.426 ml/ml. Tissue fractions of gray and white matter for the cerebellar cortex were 0.657 and 0.284 ml/ml, respectively. Averaged T1-weighted MR images and averaged images of gray and white matter fractions that were anatomically standardized are shown in Figure 3.

The relations between average tissue fraction of gray matter and average CBF values obtained with PET or SPECT (IMP, PAO, and ECD) for all ROIs except the centrum semiovale are shown in Figure 4. No significant correlations were observed.

DISCUSSION

While diffusible tracer $H_2{}^{15}O$ has been used as a gold standard to measure CBF, accumulative tracers, such as IMP, PAO, and ECD, are currently used to trace CBF in SPECT studies of the pathophysiology of neurological

diseases. Although these accumulative tracers are all characterized by a large first-pass extraction fraction in the brain tissue, the tracers are retained in the brain by different mechanisms.[4,10,11] The differences in the mechanism of retention must cause differences in regional distribution in the brain. In the present study, differences in regional distribution were observed between these accumulative tracers and between the accumulative tracers and $H_2^{15}O$ in the pons, midbrain, thalamus, putamen, parahippocampal gyrus, posterior cingulate gyrus, temporal cortex, and occipital cortex. In the brain stem, thalamus, and putamen, CBF values measured by SPECT tracers were lower than values measured by $H_2^{15}O$, indicating weak retention of SPECT tracers in these brain regions. In addition, in the thalamus and putamen, CBF values measured by SPECT tracers might be underestimated due to a limited first-pass extraction fraction in brain and a backdiffusion from brain to blood because CBF values in these regions were largest through the brain.[30-32] In the parahippocampal gyrus, CBF values measured by IMP and ECD, but not by PAO, were lower than values measured by $H_2^{15}O$, indicating weak retention of IMP and ECD in this region. In the posterior cingulate and temporal cortex, CBF values measured by SPECT tracers were lower than values measured by $H_2^{15}O$. The arterial blood volume in an ROI is relatively large in these regions,[33] and this can cause overestimation of CBF as measured by $H_2^{15}O$.[34] In the occipital cortex, CBF values measured by IMP and PAO, but not by ECD, were lower than those measured by $H_2^{15}O$, indicating weak retention of IMP and PAO in this region. Koyama et al. also reported that CBF measured by PAO was less than CBF measured by ECD in the occipital cortex.[12] In the centrum semiovale, CBF values measured by IMP and PAO were higher than CBF measured by $H_2^{15}O$ due to scatter effect in the SPECT system.[35,36] However, CBF values measured by ECD were almost the same as CBF measured by $H_2^{15}O$ in the centrum semiovale. This suggests that retention of ECD in the white matter is relatively weak. In addition, effects of attenuation and scatter in SPECT must be different between ^{123}I and ^{99m}Tc due to a difference in energy of γ-ray.

In the present study, no significant correlations were observed between average tissue fraction of gray matter and average CBF values measured by $H_2^{15}O$, IMP, PAO, or ECD, indicating that regional distribution of CBF is independent of the regional gray matter fraction. However, the CBF value is affected by the regional gray matter fraction due to a limited spatial resolution of PET and SPECT scanner. The CBF value in an ROI can be expressed as follows[17]:

$$CBF = f_{gray} \cdot TF_{gray} + f_{white} \cdot TF_{white} \qquad \text{Eq. 1}$$

where f_{gray} and f_{white} are blood flow in gray and white matter (ml/100 ml/min), respectively, and TF_{gray} and TF_{white} are the tissue fraction of gray and matter (ml/ml),

Table 4 Blood flow in gray matter calculated for each ROI according to Eq. 1

Region	PET	SPECT		
		IMP	PAO	ECD
Cerebellum	84.6	81.2	82.6	83.3
Pons	105.8	82.4	82.3	81.6
Midbrain	99.1	74.4	80.4	72.2
Thalamus	115.3	80.8	91.1	82.4
Putamen	98.1	78.0	83.3	82.2
Parahippocampal gyrus	64.8	59.4	64.7	55.8
Anterior cingulate	78.8	73.1	77.3	76.1
Posterior cingulate	97.7	75.2	79.2	79.1
Frontal cortex	89.4	88.4	87.3	87.6
Temporal cortex	90.9	79.7	76.5	77.9
Occipital cortex	110.2	94.5	90.6	105.7
Parietal cortex	85.9	80.6	79.7	82.4

Values are ml/100 ml/min

respectively. According to this equation, if f_{white} is given, f_{gray} can be calculated for a given TF_{gray} and TF_{white}, which are determined by voxel-based morphometry with MR imaging. The f_{gray} values calculated from average CBF for each ROI by assuming f_{white} to be equal to CBF value in the centrum semiovale are given in Table 4. In this calculation, TF_{gray} and TF_{white} were derived from average images of gray and white matter fractions for each ROI. Among the neocortical regions, f_{gray} ranged from 86 to 110 for $H_2^{15}O$, from 80 to 95 for IMP, from 77 to 91 for PAO, and from 78 to 106 ml/100 ml/min for ECD. This indicates that the blood flow per gray matter volume is different for each brain region, even in neocortical regions. For all tracers, the lowest and highest f_{gray} values are observed in the parahippocampal gyrus and occipital cortex, respectively.

The hippocampal region is of central interest in the complex pathophysiology of Alzheimer's disease. Hypoperfusion of the parahippocampal gyrus has been reported in the presence of mild Alzheimer's disease.[37-39] The voxel-based morphometry technique revealed gray matter loss in the hippocampal region in the presence of mild Alzheimer's disease[40,41] and mild cognitive impairment.[42] However, there is reportedly no change in perfusion of the parahippocampal gyrus in mild Alzheimer's disease,[43,44] although a decrease in gray matter volume in the parahippocampal gyrus has been observed.[44] In the present study, the greatest tissue fraction of gray matter was observed in the parahippocampal gyrus. However, CBF was not greater in this region than in the other regions for any tracer; thus this region had the lowest gray-matter blood flow values of any region (Table 4), especially in the ECD study. Such discrepancy between the gray matter fraction and CBF might affect the detectability of abnormal perfusion in the parahippocampal gyrus in cases of Alzheimer's disease.

In conclusion, a database of CBF values measured in

healthy subjects by three accumulative SPECT tracers, IMP, PAO, and ECD, was built. Differences in regional distribution of CBF were observed between tracers. Regional distribution of CBF was independent of the regional gray matter fraction measured by voxel-based morphometry with MR imaging for all tracers, and consequently, blood flow per gray matter volume was different for each brain region. In particular, the least blood flow in gray matter was observed in the parahippocampal gyrus.

ACKNOWLEDGMENTS

REFERENCES

1. Kanno I, Lassen NA. Two methods for calculating regional cerebral blood flow from emission computed tomography of inert gas concentrations. *J Comput Assist Tomogr* 1979; 3: 71–76.
2. Herscovitch P, Markham J, Raichle ME. Brain blood flow measured with intravenous $H_2^{15}O$. I. Theory and error analysis. *J Nucl Med* 1983; 24: 782–789.
3. Kanno I, Iida H, Miura S, Murakami M, Takahashi K, Sasaki H, et al. A system for cerebral blood flow measurement using an $H_2^{15}O$ autoradiographic method and positron emission tomography. *J Cereb Blood Flow Metab* 1987; 7: 143–153.
4. Winchell HS, Baldwin RM, Lin TH. Development of I-123-labeled amines for brain studies: localization of I-123 iodophenylalkyl amines in rat brain. *J Nucl Med* 1980; 21: 940–946.
5. Winchell HS, Horst WD, Braun L, Oldendorf WH, Hattner R, Parker H. N-isopropyl-[^{123}I]p-iodoamphetamine: single-pass brain uptake and washout; binding to brain synaptosomes; and localization in dog and monkey brain. *J Nucl Med* 1980; 21: 947–952.
6. Sharp PF, Smith FW, Gemmell HG, Lyall D, Evans NT, Gvozdanovic D, et al. Technetium-99m HM-PAO stereoisomers as potential agents for imaging regional cerebral blood flow: human volunteer studies. *J Nucl Med* 1986; 27: 171–177.
7. Neirinckx RD, Canning LR, Piper IM, Nowotnik DP, Pickett RD, Holmes RA, et al. Technetium-99m d,l-HM-PAO: a new radiopharmaceutical for SPECT imaging of regional cerebral blood perfusion. *J Nucl Med* 1987; 28: 191–202.
8. Walovitch RC, Hill TC, Garrity ST, Cheesman EH, Burgess BA, O'Leary DH, et al. Characterization of technetium-99m-L,L-ECD for brain perfusion imaging, part 1: pharmacology of technetium-99m ECD in nonhuman primates. *J Nucl Med* 1989; 30: 1892–1901.
9. Leveille J, Demonceau G, De Roo M, Rigo P, Taillefer R, Morgan RA, et al. Characterization of technetium-99m-L,L-ECD for brain perfusion imaging, Part 2: Biodistribution and brain imaging in humans. *J Nucl Med* 1989; 30: 1902–1910.
10. Ballinger JR, Reid RH, Gulenchyn KY. Technetium-99m HM-PAO stereoisomers: differences in interaction with glutathione. *J Nucl Med* 1988; 29: 1998–2000.
11. Walovitch RC, Cheesman EH, Maheu LJ, Hall KM. Studies of the retention mechanism of the brain perfusion imaging agent ^{99m}Tc-bicisate (^{99m}Tc-ECD). *J Cereb Blood Flow Metab* 1994; 14 Suppl 1: S4–11.
12. Koyama M, Kawashima R, Ito H, Ono S, Sato K, Goto R, et al. SPECT imaging of normal subjects with technetium-99m-HMPAO and technetium-99m-ECD. *J Nucl Med* 1997; 38: 587–592.
13. Inoue K, Nakagawa M, Goto R, Kinomura S, Sato T, Sato K, et al. Regional differences between ^{99m}Tc-ECD and ^{99m}Tc-HMPAO SPET in perfusion changes with age and gender in healthy adults. *Eur J Nucl Med Mol Imaging* 2003; 30: 1489–1497.
14. Hoedt-Rasmussen K. Regional cerebral flow in man measured externally following intra-arterial administration of ^{85}Kr or ^{133}Xe dissolved in saline. *Acta Neurol Scand Suppl* 1965; 14: 65–68.
15. Ingvar DH, Cronqvist S, Ekberg R, Risberg J, Hoedt-Rasmussen K. Normal values of regional cerebral blood flow in man, including flow and weight estimates of gray and white matter. A preliminary summary. *Acta Neurol Scand Suppl* 1965; 14: 72–78.
16. Hoedt-Rasmussen K, Sveinsdottir E, Lassen NA. Regional cerebral blood flow in man determined by intra-arterial injection of radioactive inert gas. *Circ Res* 1966; 18: 237–247.
17. Iida H, Law I, Pakkenberg B, Krarup-Hansen A, Eberl S, Holm S, et al. Quantitation of regional cerebral blood flow corrected for partial volume effect using O-15 water and PET: I. Theory, error analysis, and stereologic comparison. *J Cereb Blood Flow Metab* 2000; 20: 1237–1251.
18. Law I, Iida H, Holm S, Nour S, Rostrup E, Svarer C, et al. Quantitation of regional cerebral blood flow corrected for partial volume effect using O-15 water and PET: II. Normal values and gray matter blood flow response to visual activation. *J Cereb Blood Flow Metab* 2000; 20: 1252–1263.
19. Ashburner J, Friston KJ. Voxel-based morphometry —the methods. *Neuroimage* 2000; 11: 805–821.
20. Good CD, Johnsrude IS, Ashburner J, Henson RN, Friston KJ, Frackowiak RS. A voxel-based morphometric study of ageing in 465 normal adult human brains. *Neuroimage* 2001; 14: 21–36.
21. Good CD, Johnsrude I, Ashburner J, Henson RN, Friston KJ, Frackowiak RS. Cerebral asymmetry and the effects of sex and handedness on brain structure: a voxel-based morphometric analysis of 465 normal adult human brains. *Neuroimage* 2001; 14: 685–700.
22. Kimura K, Hashikawa K, Etani H, Uehara A, Kozuka T, Moriwaki H, et al. A new apparatus for brain imaging:

four-head rotating gamma camera single-photon emission computed tomograph [see comments]. *J Nucl Med* 1990; 31: 603–609.

23. Chang LT. A method for attenuation correction in radionuclide computed tomography. *IEEE Trans Nucl Sci* 1978; 25: 638–643.

24. Chang LT. Attenuation correction and incomplete projection in single photon emission computed tomography. *IEEE Trans Nucl Sci* 1979; 26: 2780–2789.

25. Iida H, Miura S, Kanno I, Ogawa T, Uemura K. A new PET camera for noninvasive quantitation of physiological functional parametric images: Headtome-V-dual. In: Myers R, Cunningham V, Bailey D, Jones T, eds. *Quantification of brain function using PET*. San Diego; Academic Press, 1996: 57–61.

26. Iida H, Kanno I, Miura S, Murakami M, Takahashi K, Uemura K. Error analysis of a quantitative cerebral blood flow measurement using $H_2^{15}O$ autoradiography and positron emission tomography, with respect to the dispersion of the input function. *J Cereb Blood Flow Metab* 1986; 6: 536–545.

27. Iida H, Higano S, Tomura N, Shishido F, Kanno I, Miura S, et al. Evaluation of regional differences of tracer appearance time in cerebral tissues using [^{15}O]water and dynamic positron emission tomography. *J Cereb Blood Flow Metab* 1988; 8: 285–288.

28. Raichle ME, Martin WR, Herscovitch P, Mintun MA, Markham J. Brain blood flow measured with intravenous $H_2^{15}O$. II. Implementation and validation. *J Nucl Med* 1983; 24: 790–798.

29. Friston KJ, Frith CD, Liddle PF, Dolan RJ, Lammertsma AA, Frackowiak RS. The relationship between global and local changes in PET scans. *J Cereb Blood Flow Metab* 1990; 10: 458–466.

30. Renkin EM. Transport of potassium-42 from blood to tissue in isolated mammalian skeletal muscles. *Am J Physiol* 1959; 197: 1205–1210.

31. Crone C. The permeability of capillaries in various organs as determined by use of the 'indicator diffusion' method. *Acta Physiol Scand* 1963; 58: 292–305.

32. Iida H, Akutsu T, Endo K, Fukuda H, Inoue T, Ito H, et al. A multicenter validation of regional cerebral blood flow quantitation using [^{123}I]iodoamphetamine and single photon emission computed tomography. *J Cereb Blood Flow Metab* 1996; 16: 781–793.

33. Okazawa H, Yamauchi H, Sugimoto K, Toyoda H, Kishibe Y, Takahashi M. Effects of acetazolamide on cerebral blood flow, blood volume, and oxygen metabolism: a positron emission tomography study with healthy volunteers. *J Cereb Blood Flow Metab* 2001; 21: 1472–1479.

34. Ito H, Kanno I, Iida H, Hatazawa J, Shimosegawa E, Tamura H, et al. Arterial fraction of cerebral blood volume in humans measured by positron emission tomography. *Ann Nucl Med* 2001; 15: 111–116.

35. Iida H, Narita Y, Kado H, Kashikura A, Sugawara S, Shoji Y, et al. Effects of scatter and attenuation correction on quantitative assessment of regional cerebral blood flow with SPECT. *J Nucl Med* 1998; 39: 181–189.

36. Ito H, Iida H, Kinoshita T, Hatazawa J, Okudera T, Uemura K. Effects of scatter correction on regional distribution of cerebral blood flow using I-123-IMP and SPECT. *Ann Nucl Med* 1999; 13: 331–336.

37. Kogure D, Matsuda H, Ohnishi T, Asada T, Uno M, Kunihiro T, et al. Longitudinal evaluation of early Alzheimer's disease using brain perfusion SPECT. *J Nucl Med* 2000; 41: 1155–1162.

38. Rodriguez G, Vitali P, Calvini P, Bordoni C, Girtler N, Taddei G, et al. Hippocampal perfusion in mild Alzheimer's disease. *Psychiatry Res* 2000; 100: 65–74.

39. Callen DJ, Black SE, Caldwell CB. Limbic system perfusion in Alzheimer's disease measured by MRI-coregistered HMPAO SPET. *Eur J Nucl Med Mol Imaging* 2002; 29: 899–906.

40. Frisoni GB, Testa C, Zorzan A, Sabattoli F, Beltramello A, Soininen H, et al. Detection of grey matter loss in mild Alzheimer's disease with voxel based morphometry. *J Neurol Neurosurg Psychiatry* 2002; 73: 657–664.

41. Karas GB, Burton EJ, Rombouts SA, van Schijndel RA, O'Brien JT, Scheltens P, et al. A comprehensive study of gray matter loss in patients with Alzheimer's disease using optimized voxel-based morphometry. *Neuroimage* 2003; 18: 895–907.

42. Chetelat G, Desgranges B, De La Sayette V, Viader F, Eustache F, Baron JC. Mapping gray matter loss with voxel-based morphometry in mild cognitive impairment. *Neuroreport* 2002; 13: 1939–1943.

43. Ishii K, Sasaki M, Yamaji S, Sakamoto S, Kitagaki H, Mori E. Paradoxical hippocampus perfusion in mild-to-moderate Alzheimer's disease. *J Nucl Med* 1998; 39: 293–298.

44. Kitayama N, Matsuda H, Ohnishi T, Kogure D, Asada T, Uno M, et al. Measurements of both hippocampal blood flow and hippocampal gray matter volume in the same individuals with Alzheimer's disease. *Nucl Med Commun* 2001; 22: 473–477.